Haji Haji, V., Fekih, A., Monje, C. A. & Fakhri Asfestani, R. (2020). Adaptive model predictive control design for the speed and temperature control of a V94.2 gas turbine unit in a combined cycle power plant. *Energy, 207*, 118259.

DOI: 10.1016/j.energy.2020.118259

Adaptive model predictive control design for the speed and temperature control of a V94.2 gas turbine unit in a combined cycle power plant

Vahab Haji Haji[a,*], Afef Fekih[b], Concepción Alicia Monje[c], Ramin Fakhri Asfestani[d]

[a] *Young Researchers and Elite Club, Borujerd Branch, Islamic Azad University, Borujerd, Iran*
[b] *Electrical and Computer Engineering Department, University of Louisiana at Lafayette, Lafayette, LA 70504, USA*
[c] *Systems Engineering and Automation Department, University Carlos III of Madrid, Avenida Universidad 30, 28911 Leganés, Madrid, Spain*
[d] *Power Plant Monitoring and Control Research Department, Niroo Research Institute, Tehran, Iran*

Abstract

This paper proposes an adaptive model predictive control (AMPC) approach with online parameter estimation for a V94.2 gas turbine mounted in the Damavand combined cycle power plant (CCPP). The AMPC is designed to simultaneously maintain the speed and temperature responses of the gas turbine within their desired levels in the presence of frequency drop or change in load demand. It implements an online parameter estimation and adaptive mechanism to enable the model parameters to follow any change in the V94.2 gas turbine power plant (GTPP) model and provide the best control performance possible. The effectiveness of the AMPC approach is assessed using an estimated model of a V94.2 gas turbine mounted in the Damavand CCPP. Additional analysis is also performed via a comparison study encompassing a classical MPC, H_∞, and $\mu - synthesis$ robust control strategies and considering reference tracking performance, transient and steady-state responses, disturbance rejection capabilities, and robustness to parameter

*Corresponding author. Address:
Tel.: +98 936 54 75 525;Fax: +98 66 42605335.
Email address: vhbhaji@gmail.com (Vahab Haji Haji)

variations. The obtained results confirmed the effectiveness of the proposed approach in improving the robust stability and dynamics of the V94.2 GTPP in the presence of measurement noise, frequency disturbance, and unmodeled power plant dynamics along with its superior performance in terms of tracking capability and disturbance rejection properties.

Keywords: V94.2 gas turbine, adaptive model predictive control, robust control, H_∞, $\mu - synthesis$.

---

1. Introduction

Gas turbines are widely used in a variety of aero, marine and industrial applications. Attributes such as high efficiency, fast start up, and flexibility in fuel selection make single-shaft or twin-shaft gas turbines an appropriate choice for electrical power generation [1, 2]. However, accurately modeling and controlling the gas turbine so as to properly mitigate frequency and load transients and ensure good tracking performance are key issues that require more consideration and efforts to be devoted.

The control system is a vital part of a gas turbine power plant (GTPP). Without an appropriate control law, any change in power demand or deviation in frequency can lead to overheating or over speeding, and even system shutdown. To improve the stability of a gas turbine power plant, Eslami et. al. [3] proposed an intelligent method, based on the artificial bee colony (ABC) algorithm, to design an optimal PID-based low-pass filter for a gas turbine power plant to improve its stability. The proposed controller was able to improve the dynamic performance of the gas turbine in different operating conditions. It also resulted in fuel consumption saving compared to a PID controller tuned by particle swarm optimization (PSO) algorithm and genetic algorithm (GA). A fractional-order fuzzy-PID controller was proposed in [4] to enhance the combined cycle power plant (CCPP) temperature and frequency responses. Compared to the simple PID controller, the proposed fractional-order fuzzy-PID controller had more flexibility and was able to simultaneously improve the transient and steady-state responses of the CCPP. The authors used the PSO algorithm to tune the controller gains. The performance of the proposed controller was considered in terms of frequency drop and changes in power demand and compared to those controllers tuned by PSO, GA, differential evolution (DE), and ABC algorithms. However, the limitations of PID-based controllers, especially for multivariable constrained

systems, are very well documented in the literature [5].

Model predictive control (MPC) has proven to be very effective in dealing with large multivariable constrained control systems [6]. Its simplicity, ease of implementation and accurate tracking performance have led to its successful implementation in various industrial applications and its recent adoption in power and energy systems [7, 8]. For instance, in [9] an MPC approach was proposed to optimize the energy production of an inertial sea wave energy converter while satisfying a set of constraints such as speed limitation, control effort, and energy production requirements. A hierarchical model predictive control was proposed in [10] to maintain the frequency stability of a wind farm during black-start in the energy storage system. The proposed controller was evaluated under both low and high wind conditions. Shan and Wang proposed an MPC control strategy to control the charging/discharging of a thermal energy storage system. The approach was able to improve the efficiency of the system up to 22.94 % [11]. A model predictive control (MPC) strategy was proposed in [12] for a gas turbine power plant. The authors used an autoregressive with exogenous input (ARX) identification approach to estimate a linear time-invariant model for a GE9001E gas turbine power plant. Based on the estimated model, an MPC controller was designed and implemented to adjust the speed and temperature loops in a desired interval. Though the controller showed superior performance to conventional PID and a SpeedTronic controllers, its robust stability and performance in the presence of any frequency drop or model uncertainty has not been considered.

In a CCPP, the performance of gas and steam turbines are highly dependent on the control strategy. In the absence of an appropriate controller, any frequency drop or load demand variation can negatively affect the performance of the power plant and can damage the power plant units, even leading to power grid instability and blackouts. Besides, there are usually lots of discrepancies between the dynamics of the real gas turbine and the modeled dynamics, which can deteriorate the performance of any classical (PID), heuristic (PSO-, GA-, ABC-based), and MPC ([6]) controllers. Therefore, in designing controllers, the robust stability and performance of the systems in the presence of frequency disturbance, measurement noise, and unmodeled power plant dynamics demand much more attention and priorities. In these conditions, the adaptive model predictive controller (AMPC) seems to be a more appropriate choice, since it uses online parameter estimation to follow any change in the physical system and update the control rules based on the

new estimated model to ensure the best and most effective control strategy.

Based on the above discussion, we propose in this paper an adaptive MPC strategy for both the temperature and speed control loops of a V94.2 gas turbine unit mounted in the Damavand power plant. The main contributions of this paper are twofold:

- Design and implementation of AMPC controllers for the speed and temperature loops of a V94.2 gas turbine.
- A comparison analysis between the performance of the AMPC and those of the MPC, H_∞, and $\mu - synthesis$ controllers in terms of tracking performance, steady-state and transient responses, and robustness to uncertainties.

The remainder of the paper is organized as follows. The mathematical model of a gas turbine is presented in section 2. Section 3 is devoted to the description of the V94.2 gas turbine power plant linear ARX model. The MPC formulations for the gas turbine power plant and the basic idea of the AMPC strategy are provided in section 4. Section 5 is dedicated to the comparative study, discussion, and simulation results. Finally, section 6 presents some concluding remarks.

2. Gas turbine power plant mathematical model

Various models aiming at either providing an accurate representation of the gas turbine's response, or analyzing the ambient temperature effect on the power output, or studying the impact of the gas turbine dynamics on frequency drop have been provided in the literature. In [13], a simplified mathematical model of a heavy-duty gas turbine power plant was proposed by Rowen. This model is useful in dynamic power system and connected equipment studies and analyses. The model was extended in another work by Rowen to show the impact of the ambient temperature and Inlet Guide Vane (IGV) in power and temperature outputs [14]. Kunitomi et. al. used Rowen's model as a starting point for the development of an appropriate model to determine the frequency dependency of gas turbine output [15]. A small and large signal modeling of a gas turbine power plant for load frequency control study was proposed in [16]. In [17], the authors used a gray box method to provide a dynamic model for an industrial gas turbine (Qeshm power plant) in loading and unloading conditions.

Gas turbine, compressor and combustion chamber are three main components of a typical gas turbine power plant. The compressed air burns with fuel in the combustor to produce a high temperature and pressure gas. This high pressure and temperature gas drives the gas turbine and the generator to provide mechanical and electrical power. A simplified gas turbine block diagram including temperature and speed loops is depicted in Fig. 1. The input/output signals are summarized in Table 1 [1]. In Fig. 1, the main control signals are: 1) W_f (fuel flow) and 2) IGV(inlet guide vanes) or W_a, and the main output signals are: 1) T_e (exhaust temperature), 2) P_m (power demand), and 3) N (rotor speed or frequency).

As Fig. 1 shows (red line), the speed or frequency loop includes the speed controller (governor), fuel limits, fuel system and components, gas turbine, and rotor dynamics. The speed controller follows the output speed (frequency) and changes the fuel supply to compensate for any frequency deviation.

As Fig. 1 shows (green line), the temperature loop includes a normal and an overheat temperature control branches. The overheat controller, fuel limits, gas fuel system, combustor, and temperature transducer are the main components of the overheat temperature branch. The main task of this branch is to prevent turbine overloading and severe overheating. The normal temperature branch mainly acts using the IGV controller (air system) and the actuator to 1) prevent the exhaust temperature T_e from exceeding the temperature reference T_r, and 2) modulate temperature at its maximum level for part load optimization or heat recovery applications [13].

For a gas turbine process, the existing relationships and equations between inputs and outputs are defined by [1, 18]:

$$T_f = T_d + (T_{f0} - T_{d0}) \frac{W_f}{W_a}, \tag{1}$$

$$x = (Q_{r0} W_a)^{\frac{\gamma-1}{\gamma}}, \tag{2}$$

$$T_d = T_a \left(1 + \frac{x-1}{\eta_c}\right), \tag{3}$$

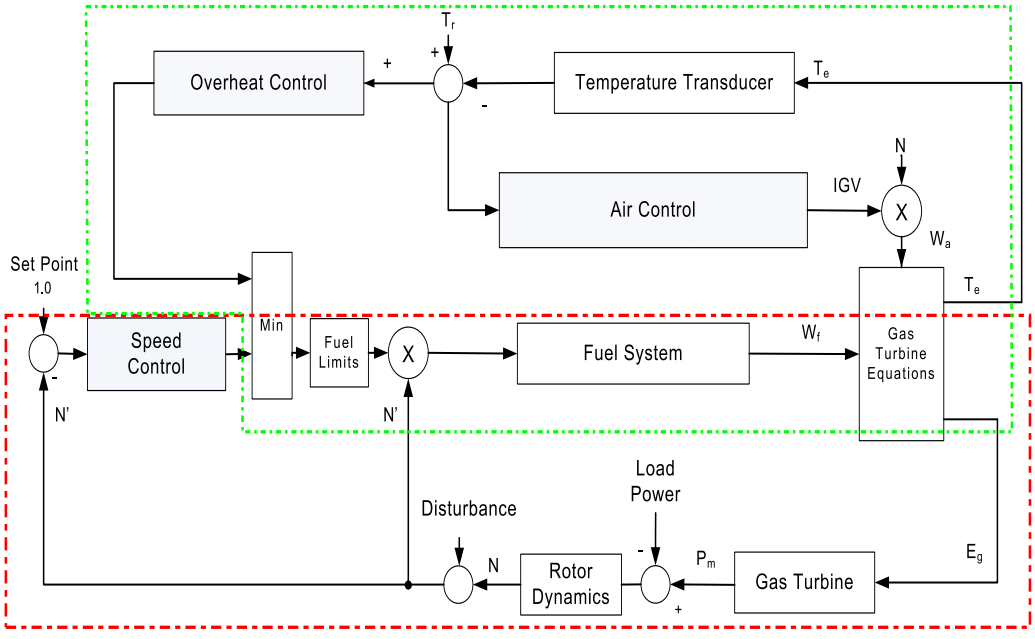

Figure 1: Gas turbine power plant block diagram

where T_{f0}, T_{d0}, x, P_{r0}, γ, η_c are described in Table 1. The temperature T_e and energy supplied to the gas turbine can be expressed as follows:

$$T_e = T_f \left[1 - \left(1 - \frac{1}{x}\right)\eta_t\right], \tag{4}$$

$$E_g = K_0 \left\{(T_f - T_e) - (T_d - T_a)\right\} W_a, \tag{5}$$

where η_t is the turbine efficiency. More details about the GTPP's model, signals, and parameters can be found in [1, 4, 18, 19].

3. V94.2 gas turbine linear model

In what follows, we will adopt the identified linear model provided in our previous work [1]. The linear model is based on the real-time data for the V94.2 gas turbine unit mounted in the Damavand power plant, and it can follow the plant outputs with a sufficient accuracy. The autocorrelation of residuals, transient and steady-state diagrams for gas turbine response, and

Table 1: Gas turbine main input and output signals

Signals	**D**efinition
P_m	Gas turbine generated power (pu)
P_d	Power demand (pu)
E_g	Thermal power converted by the gas turbine
T_e	Exhaust temperature (pu)
T_r	Reference temperature (pu)
T_a	Ambient temperature (^oC)
T_f	Gas turbine inlet temperature (pu)
F_l	Fuel demand signal (pu)
N	Rotor speed (frequency)
W_a	Air flow
W_f	Fuel flow (pu)
IGV	Inlet guide vanes
T_{f0}	Rated value for the gas turbine inlet temperature (^oC)
T_{d0}	Rated value for the compressor discharge temperature (^oC)
x	Compressor temperature ratio
η_t	Turbine efficiency
P_{r0}	Nominal compressor pressure ratio
γ	Ratio of specific heats
η_c	Compressor efficiency
K_0	Gas turbine coefficient

fitness percentage have been used to assess the performance of the estimated model.

For the Damavand V94.2 GTPP, the base load is $115MW$, the ambient temperature is around 30^oC or 303^oK, the atmospheric pressure is 896.5mbar, IGV is between 0.52 and 1, N is 0.95 to 1, and F_l is $[0, 1.0]$. These data are provided for no-load to full-load conditions with sampling time of 1sec.

For this model, the value of the mean square normalized error performance function (MSE), Akaike's final prediction error (FPE), and fitness percentage (Fit) for the speed loop are 1.917×10^{-04}, 1.927×10^{-04}, and 92.72%, respectively. Similarly, for the temperature loop, MSE, FPE, and Fit are 1.161×10^{-05}, 1.179×10^{-05}, and 94.7%, respectively [1].

Figure 2 shows the block diagram of the estimated ARX model for the V94.2 gas turbine power plant where, for speed loop, the fuel flow F_l, N, T_a, power demand P_d, and IGV are inputs variables, whereas P_m is the output signal. Similarly, for the temperature loop, F_l, N, T_a, and IGV are inputs signals, and temperature T_e is the output. The identified transfer functions between T_e and P_m as outputs, and T_a, N, IGV and F_l as inputs are as

follows [1]:

$$G_1(s) = \frac{P_m(s)}{F_l(s)} = \frac{0.65s^3 + 0.46s^2 + 0.569s + 0.0412}{s^4 + 0.988s^3 + 2.208s^2 + 0.645s + 0.033}, \tag{6}$$

$$G_2(s) = \frac{P_m(s)}{N(s)} = \frac{-2.121s^3 - 2.896s^2 - 1.94s - 0.017}{s^4 + 0.988s^3 + 2.208s^2 + 0.645s + 0.033}, \tag{7}$$

$$G_3(s) = \frac{1}{14.5s}, \tag{8}$$

$$G_4(s) = \frac{P_m(s)}{T_a(s)} = \frac{-0.008s^3 + 0.001s^2 - 0.003s + 2.756 \times 10^{-05}}{s^4 + 0.988s^3 + 2.208s^2 + 0.645s + 0.033}, \tag{9}$$

$$G_5(s) = \frac{P_m(s)}{IGV(s)} = \frac{0.061s^3 + 0.071s^2 + 0.115s + 0.00071}{s^4 + 0.988s^3 + 2.208s^2 + 0.645s + 0.033}, \tag{10}$$

$$G_6(s) = \frac{T_e(s)}{N(s)} = \frac{13.22s + 0.050}{s^2 + 6.31s + 0.096}, \tag{11}$$

$$G_7(s) = \frac{T_e(s)}{T_a(s)} = \frac{-0.025s - 5.32 \times 10^{-05}}{s^2 + 6.31s + 0.096}, \tag{12}$$

$$G_8(s) = \frac{T_e(s)}{F_l(s)} = \frac{1.45s + 0.094}{s^2 + 6.31s + 0.096}, \tag{13}$$

$$G_9(s) = \frac{T_e(s)}{IGV(s)} = \frac{-1.34s - 0.028}{s^2 + 6.31s + 0.096}. \tag{14}$$

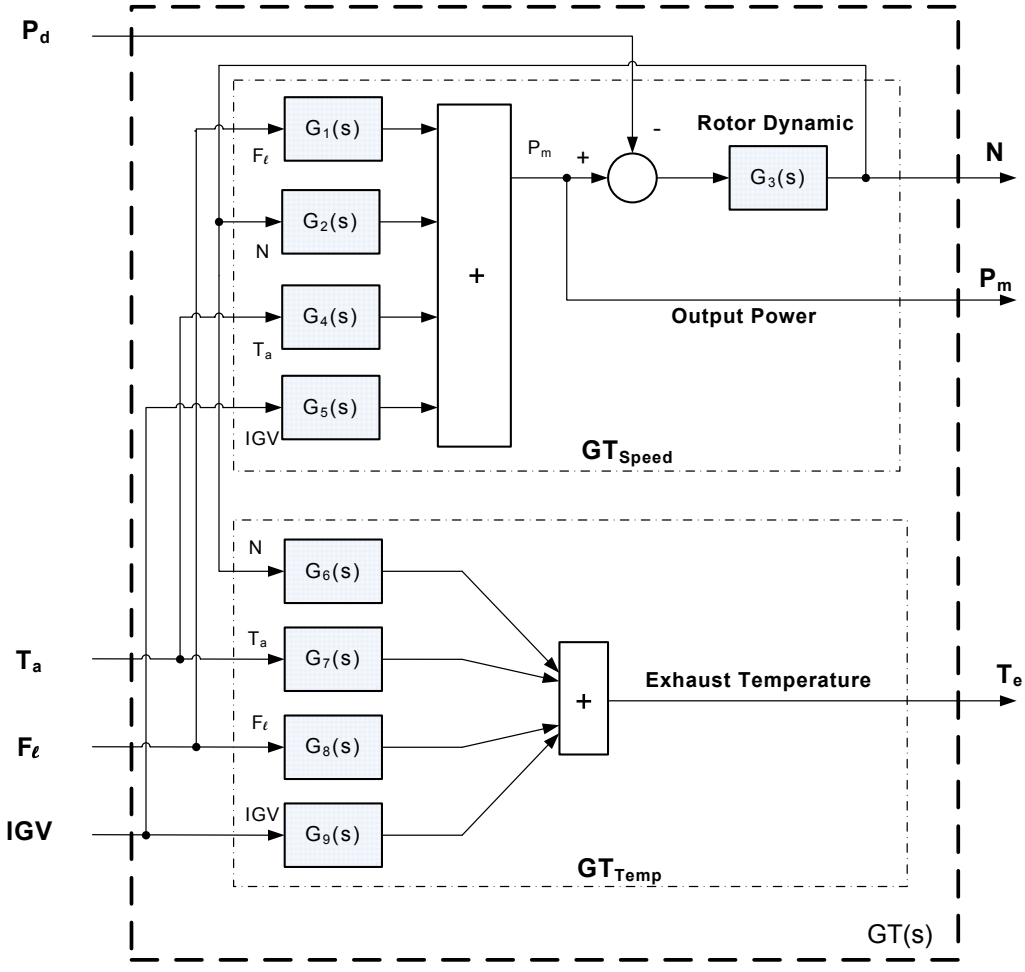

Figure 2: Estimated linear V94.2 gas turbine block diagram

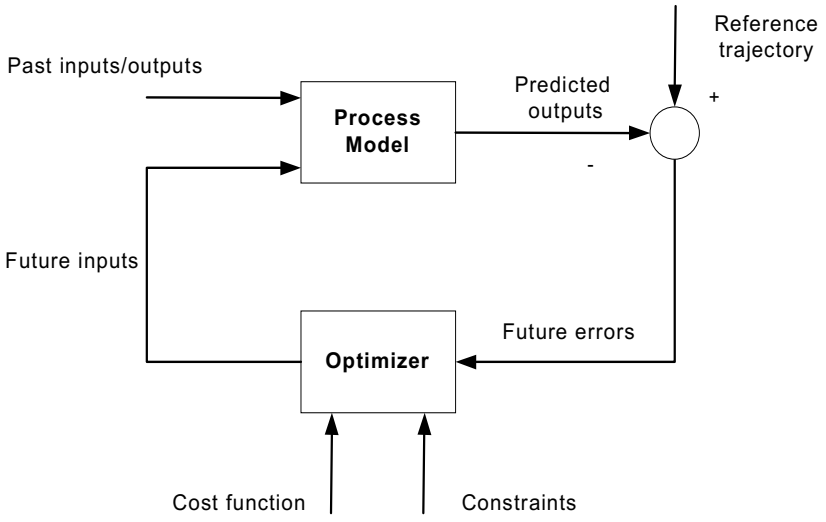

Figure 3: Basic block diagram of a MPC

4. Model predictive control

The MPC has different structures and has proven its performance using steady-state or dynamic models alike. Fig. 3 highlights the basic principle of model-based predictive control. Here, the optimizer uses the process model to predict the future plant outputs for a determined prediction horizon P and the future errors to calculate the best control actions for a determined control horizon M by minimizing of a cost function in the presence of equality/inequality constraints. The truncated impulse response model, step response model, state space model, and transfer function model are the main models to capture the process dynamics and predict the future outputs. The quadratic cost function is a choice that can be used by the optimizer to provide an appropriate control signal by taking into account the past inputs/outputs and the reference trajectory [20].

The general block diagram of a closed-loop process including the target value r, control signal u and measured output y_m is depicted in Fig. 4. In this figure, v, d, $y^{'}$, and z are measured disturbance, unmeasured disturbance, process output and measured noise, respectively [21]. The process can be described using the state-space variables of $x(k)$ as follows:

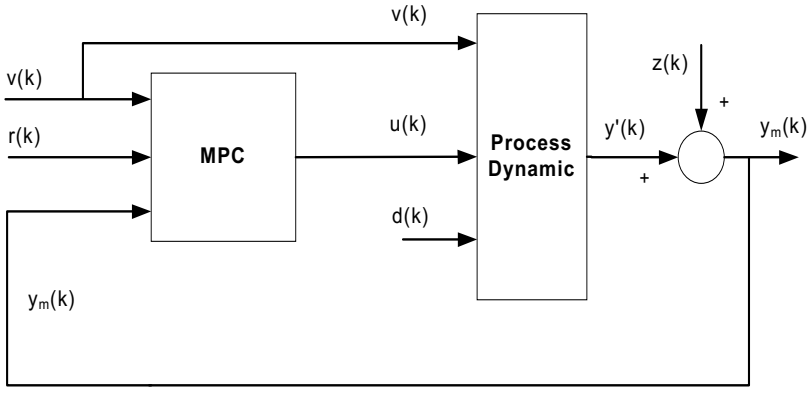

Figure 4: General block diagram of an MPC application

$$\begin{aligned} x(k+1) &= Ax(k) + B_u u(k) + B_v v(k) + B_d d(k), \\ y_m(k) &= C_m x(k) + D_{vm} v(k) + D_{dm} d(k), \\ y_u(k) &= C_u x(k) + D_{vu} v(k) + D_{du} d(k) + D_{uu} u(k), \end{aligned} \tag{15}$$

where A, B, C, D are time-invariant coefficients, and $y_m(k)$ and $y_u(k)$ are measured and unmeasured outputs, respectively. The final output $y(k)$ is the summation of $y_m(k)$ and $y_u(k)$.

The unmeasured disturbance $d(k)$ and measured noise model $m(k)$ can be defined using the Eqns. 16 and 17, respectively.

$$\begin{aligned} x_d(k+1) &= \bar{A} x_d(k) + \bar{B} n_d(k), \\ d(k) &= \bar{C} x_d(k) + \bar{D} n_d(k), \end{aligned} \tag{16}$$

$$\begin{aligned} x_m(k+1) &= \tilde{A} x_m(k) + \tilde{B} n_m(k), \\ m(k) &= \tilde{C} x_m(k) + \tilde{D} n_m(k), \end{aligned} \tag{17}$$

where $n_d(k)$ and $n_m(k)$ are the random Gaussian noises. In the case that some state variables of the process model are not measurable, the process model states $x(k)$, input/output disturbance model states $x_d(k)$ and measurement

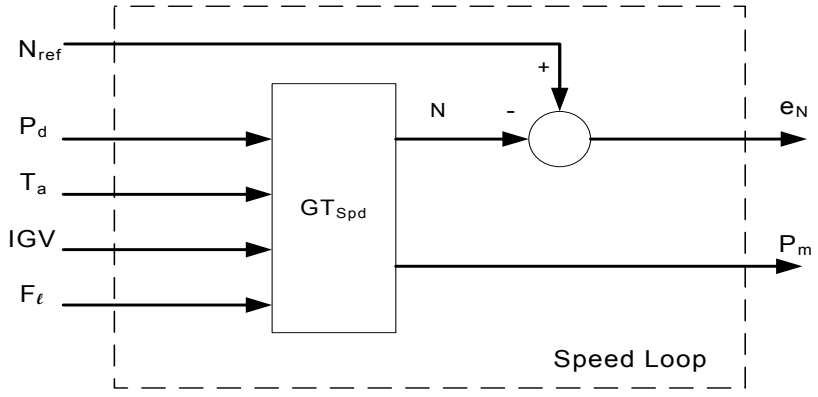

Figure 5: Block diagram for the speed loop

noise model states $x_m(k)$ can be estimated by a state observer including a Kalman filter as follows [21]:

$$\begin{bmatrix} \hat{x}(k|k) \\ \hat{x}_d(k|k) \\ \hat{x}_m(k|k) \end{bmatrix} = \begin{bmatrix} \hat{x}(k|k-1) \\ \hat{x}_d(k|k-1) \\ \hat{x}_m(k|k-1) \end{bmatrix} + M(y_m(k) - \hat{y}_m(k)), \tag{18}$$

$$\begin{bmatrix} \hat{x}(k+1|k) \\ \hat{x}_d(k+1|k) \\ \hat{x}_m(k+1|k) \end{bmatrix} = \begin{bmatrix} A\hat{x}(k|k) + B_u u(k) + B_v v(k) + B_d \bar{C}\hat{x}_d(k|k) \\ \bar{A}\hat{x}_d(k|k) \\ \tilde{A}\hat{x}_m(k|k) \end{bmatrix}, \tag{19}$$

$$\hat{y}_m(k) = C_m\hat{x}(k|k-1) + D_{vm}v(k) + D_{dm}\bar{C}\hat{x}_d(k|k-1) + \tilde{C}\hat{x}_m(k|k-1), \tag{20}$$

where $\hat{x}(k|k)$ denotes the estimation of $x(k)$ at sample time k, and here, M is calculated using Kalman filter method.

The block diagram of the speed loop is presented in Fig. 5. Based on this figure, Fig. 2, and the estimated linear transfer functions of Eqns. 6-10 for the speed loop, the system GT_{Spd} (Fig. 5) can be defined as:

$$H_1(s) = \frac{N(s)}{P_d(s)} = \frac{-G_3(s)}{1 - G_2(s)G_3(s)}, \tag{21}$$

$$H_2(s) = \frac{N(s)}{T_a(s)} = \frac{G_4(s)G_3(s)}{1 - G_2(s)G_3(s)}, \tag{22}$$

$$H_3(s) = \frac{N(s)}{IGV(s)} = \frac{G_5(s)G_3(s)}{1 - G_2(s)G_3(s)}, \tag{23}$$

$$H_4(s) = \frac{N(s)}{F_l(s)} = \frac{G_1(s)G_3(s)}{1 - G_2(s)G_3(s)}, \tag{24}$$

Eqns. 21-24 can be combined and rewritten in the form of a discrete-time state-space model with coefficients A, B, C, and D as follows:

$$\begin{aligned}
A &= \begin{bmatrix} 0.966 & -0.056 & 0.123 & -0.187 & -0.014 \\ 0.103 & 0.838 & -0.333 & 0.303 & 0.117 \\ -0.034 & 0.137 & 1.046 & -0.089 & -0.008 \\ -0.067 & -0.133 & 0.053 & 0.925 & 0.006 \\ -0.106 & 0.301 & 0.051 & -0.040 & 0.958 \end{bmatrix}, \\
B &= \begin{bmatrix} 0.055 & 9.453 \times 10^{-05} & -0.001 & -0.013 \\ 0.028 & 5.023 \times 10^{-04} & 0.0054 & 0.022 \\ -0.002 & -0.001 & 0.009 & 0.017 \\ 2.744 \times 10^{-04} & 4.997 \times 10^{-04} & 0.011 & -0.028 \\ 0.004 & -0.002 & -0.002 & -0.006 \end{bmatrix}, \\
C &= \begin{bmatrix} -0.154 & -0.165 & 0.079 & -0.017 & -0.113 \end{bmatrix}, \\
D &= \begin{bmatrix} 0 & 0 & 0 & 0 \end{bmatrix}.
\end{aligned} \tag{25}$$

where the sampling time is 0.20 sec, prediction horizon $P = 10$, control horizon $M = 3$, $0.95 < N < 1.05$, $0.1 < F_l < 1.0$, and the main model inputs are P_d, T_a, IGV, and F_l, and model output is N.

Similarly, the block diagram for the temperature loop is presented in Fig. 6. Based on this figure, Fig. 2, and the identified linear ARX model for the temperature loop (Eqns. 11-14), the system GT_{Tmp} can be defined in the form of a discrete-time state-space model as follows:

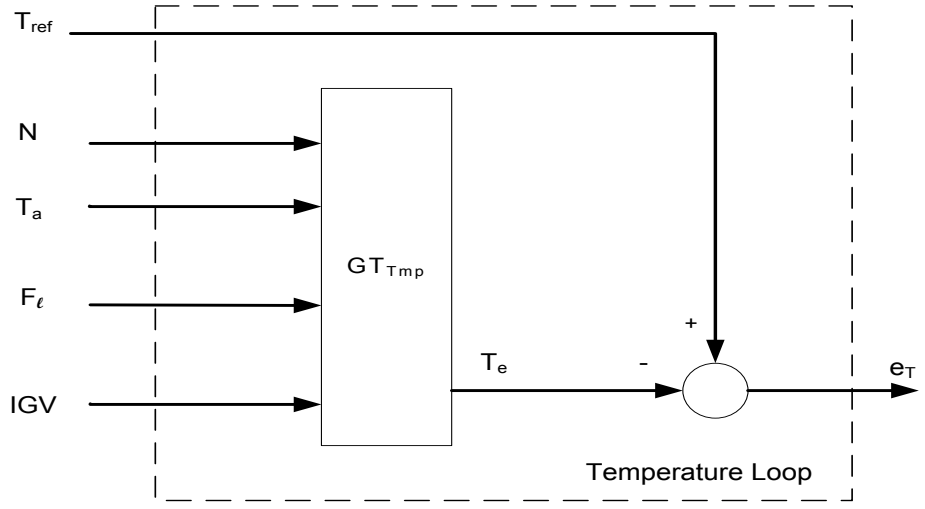

Figure 6: Block diagram for the temperature loop

$$
\begin{aligned}
A &= \begin{bmatrix} 0.999 & -0.0434 \\ 0.028 & 0.282 \end{bmatrix}, \\
B &= \begin{bmatrix} -0.007 & 2.166 \times 10^{-05} & 0.017 & -0.004 \\ 0.376 & -7.016 \times 10^{-04} & 0.041 & -0.038 \end{bmatrix}, \\
C &= \begin{bmatrix} 0 & 4 \end{bmatrix}, D = \begin{bmatrix} 0 & 0 & 0 & 0 \end{bmatrix},
\end{aligned} \tag{26}
$$

where the sampling time is 0.20 sec, prediction horizon $P = 10$, control horizon $M = 5$, $0.52 < IGV < 1.0$, and the main model inputs are N, T_a, F_l and IGV, and model output is T_e.

4.1. Adaptive model predictive control and online estimation

MPC control technique predicts the future behavior of the physical process by a linear discrete time-invariant model. Although this model is effective for many applications, to calculate the best control moves, in practice, the physical system can show a strong nonlinearity and its dynamic properties can change slowly or fastly with the time [21, 22]. In this condition, the prediction process could be inaccurate and lead to an unacceptable MPC performance.

It is worth noting that the AMPC controller uses an online estimator to control and follow the system dynamic behavior as closely as possible. The

AMPC control uses a fixed LTI discrete-time, state-space model structure as base, but allows the model parameters to evolve with the time. At the beginning of each control interval, the AMPC uses the estimated model to update the current conditions. The AMPC controller uses Kalman filter (KF) to estimate an appropriate model in the presence of output disturbance or measurement noise. The main duty of the KF is to follow any change and uncertainty in the model and provide a model state for the AMPC controller [21].

In this paper, the AMPC is used to compensate for any difference between the estimated linear gas turbine power plant model and the main physical process dynamic by changing the operating conditions. A simple block diagram for the AMPC applied to a gas turbine power plant is depicted in Fig. 7. An AMPC can be considered as a MPC controller with online parameter estimation, where plant parameters are estimated based on the measured input/output signals, and used by the MPC to compute the future control moves.

An AMPC controller uses a linear V94.2 GTPP model at the nominal operating point and, as time evolves, this model updates by an online parameters estimator. This estimator uses Eqn. (27) to estimate a multi-inputs single-output (MISO) ARX model for V94.2 GTPP mode based on the measured input/output signals.

$$A(q)y(t) = B(q)u(t - nk) + e(t), \tag{27}$$

where q, nk, $u(t)$, $y(t)$, and $e(t)$ are time-shift operator, delay, inputs, output, and the error, respectively. In this paper, for speed loop, $A(q)$ and $B(q)$ can be defined as follows:

$$\begin{aligned} A(q) &= 1 + a_1 q^{-1} + a_2 q^{-2} + a_3 q^{-3} + a_4 q^{-4} + a_5 q^{-5}, \\ B(q) &= b_1 + b_2 q^{-1} + b_3 q^{-2} + b_4 q^{-3} + b_5 q^{-4}, \end{aligned} \tag{28}$$

where $B(q)$ has four rows, and a and b are estimated coefficients, and at the start of simulation, they will be initialized to the transfer function coefficients of Eqn. 25 as follows:

$$A = \begin{bmatrix} -4.733 & 9.026 & -8.673 & 4.201 & -0.821 \end{bmatrix},$$

$$B = \begin{bmatrix} -0.014 & 0.052 & -0.073 & 0.047 & -0.011 \\ -1.052 \times 10^{-05} & 2.191 \times 10^{-05} & -2.535 \times 10^{-06} & -1.887 \times 10^{-05} & -1.002 \times 10^{-05} \\ 8.455 \times 10^{-05} & -1.449 \times 10^{-04} & -2.031 \times 10^{-05} & 1.474 \times 10^{-04} & -6.779 \times 10^{-05} \\ 8.765 \times 10^{-04} & -0.002 & -7.048 \times 10^{-05} & 0.002 & -7.461 \times 10^{-04} \end{bmatrix}. \quad (29$$

Similarly, for the temperature loop we have:

$$\begin{aligned} A(q) &= 1 + a_1 q^{-1} + a_2 q^{-2}, \\ B(q) &= b_1 + b_2 q^{-1}, \end{aligned} \quad (30)$$

where $B(q)$ has four rows, and at the start of simulation, they will be initialized to the transfer function coefficients of Eqn. 26 as follows:

$$A = \begin{bmatrix} -1.281 & 0.283 \end{bmatrix},$$

$$B = \begin{bmatrix} 1.502 & -1.501 \\ -0.003 & 0.003 \\ 0.166 & -0.163 \\ -0.152 & 0.152 \end{bmatrix}. \quad (31)$$

In the case of the gas turbine's speed loop, P_d, T_a, IGV, F_l and N are used by an online parameters estimator to follow the parameters' changes. Similarly, for temperature loop, the inputs/output N, T_a, F_l, IGV and T_e are used for the estimation process. For both speed and temperature loops, the updating frequency for online parameter estimator is 0.2 sec.

5. Results and discussions

The performance of the AMPC controllers is assessed in this section using an estimated model for V94.2 gas turbine unit mounted in Damavand combined cycle power plant. Further assessment is also carried out using a comparison study and analysis with the performance of a classical MPC, a H_∞ and $\mu - synthesis$ controllers. The robust structures and weighting functions used for H_∞ and $\mu - synthesis$ controllers are based on those presented in [1]. Details about the performance, robustness, frequency and temperature responses of these approaches can be found in [1].

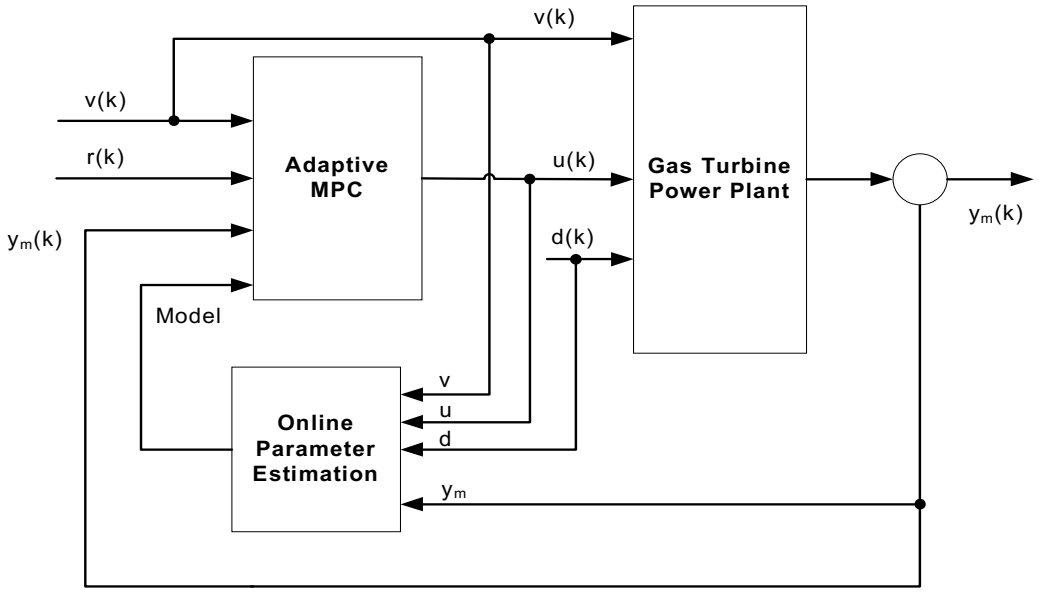

Figure 7: AMPC block diagram

In this paper, two major simulation scenarios (tracking and measurement disturbance rejection) with three levels of model uncertainties are used to assess the controller's performance under different operating conditions. Reference tracking, steady-state and transient responses, robust performance in the presence of low/high model uncertainties, and measurement disturbance rejection are the key points of these evaluations. In the first scenario, tracking scenario, the aim is to evaluate the steady-state and transient responses of the V94.2 gas turbine plant for changes in the power demand; the speed reference $N_{ref} = 1$ and $T_{ref} = 1$; after 1450 sec, P_d goes from 0.65 (pu) to 0.78 (pu); and after 650 sec, returns to 0.68 (pu). In the second scenario, disturbance rejection, the aim is to evaluate the transient response of the gas turbine unit for any frequency drop; the speed reference $N_{ref} = 1$, $T_{ref} = 1$, $P_d = 0.76$; after 3000 sec, 1% frequency drop is applied to the plant. These two scenarios are considered in the three cases of 1) under normal conditions (without model uncertainties), 2) in the presence of a low levels of model uncertainties, and 3) in the presence of high levels of model uncertainties.

5.1. Nonlinear gas turbine response under nominal conditions

The dynamic responses and optimum time indices of the V94.2 gas turbine model for the AMPC controllers compared with the MPC, H_∞ and $\mu - synthesis$ controllers are provided in Fig. 8 and Tables 2 and 3, respectively. Here M_P, T_r (sec), and T_s (sec) are the maximum peak, rise time, and settling time, respectively. ISE, IAE, ITSE, ITAE refers to integral squared error, integral absolute error, integral time squared error, and integral time absolute error [23].

In terms of tracking ability, as Fig. 8 and Table 2 shows, AMPC and MPC controllers provide the best rise time and settling time for temperature output compared with other controllers. Also, in Table 3, AMPC presents the best IAE and ITAE error for speed output. In the case of other outputs, power and T_e, this controller gives a similar results compared with the MPC, H_∞, and $\mu - synthesis$. As Table 3 shows, H_∞ controller provides the lowest ISE, IAE, ITSE, and ITAE output errors for power demand. This superiority of H_∞ controller is in close connection with the robust performance of this controller and the priority in weighting functions and control design objectives for providing the best speed and power outputs. In a GTPP, for any change in power demand, the speed controller acts to compensate any deviation in speed (frequency) output. This reaction, as Fig. 8 shows, leads to an overshoot in the fuel control signal. The impact of this sudden change in fuel flow, as Fig. 8 and Table 2 show, can be seen in all AMPC, MPC, and especially in H_∞, $\mu - synthesis$ controllers. A lower overshoot for AMPC and MPC controller in fuel demand can lead to energy saving for V94.2 GTPP compared to other controllers. As Table 3 shows, this sudden reaction and change in speed loop can enable the AMPC, MPC and H_∞ controllers to compensate for any frequency deviation as soon as possible. In Fig. 8, near time 1600 sec, the IGV controller acts through the air flow system to prevent exhausted temperature from exceeding the reference temperature of 1. In this case, the $\mu - synthesis$ controller provides the worst maximum overshoot, rise time, and settling time (Table 2). Based on Table 3, a noticeable result is that all controllers provide acceptable performance for temperature and speed outputs.

In a GTPP, it is importance to evaluate the performance of the designed controllers in the presence of output disturbances; this is mainly because any unwanted change and frequency drop can negatively affect the power plant and power network stability. Figure 9 and Table 4 show the dynamic GTPP responses for a 1٪ instantaneous frequency deviation. In Fig. 9 and

Table 4, AMPC provides the best fuel control signal and power output among three other controllers. The superiority of AMPC for effective control of fuel flow can provide a lower overshoot in temperature and power outputs. As this figure shows, in time 3000 sec for a change in speed output, the speed controller increases the fuel flow to compensate for this frequency deviation. Although the quick reaction of H_∞ controller yields a better result in terms of speed output (Table 4), it can lead to a big overshoot in the temperature and power outputs, and fuel and IGV control signals. Note also that though, $\mu - synthesis$ presents the best IGV control signal, its performance in terms of output temperature control is the worst amongst all controllers. In Fig. 9, in the case of H_∞, we can clearly see an inverse relationship between control performance for power and fuel signals, from one side, and speed output, from the other side, where a higher fuel flow can lead to a lower deviation for frequency output.

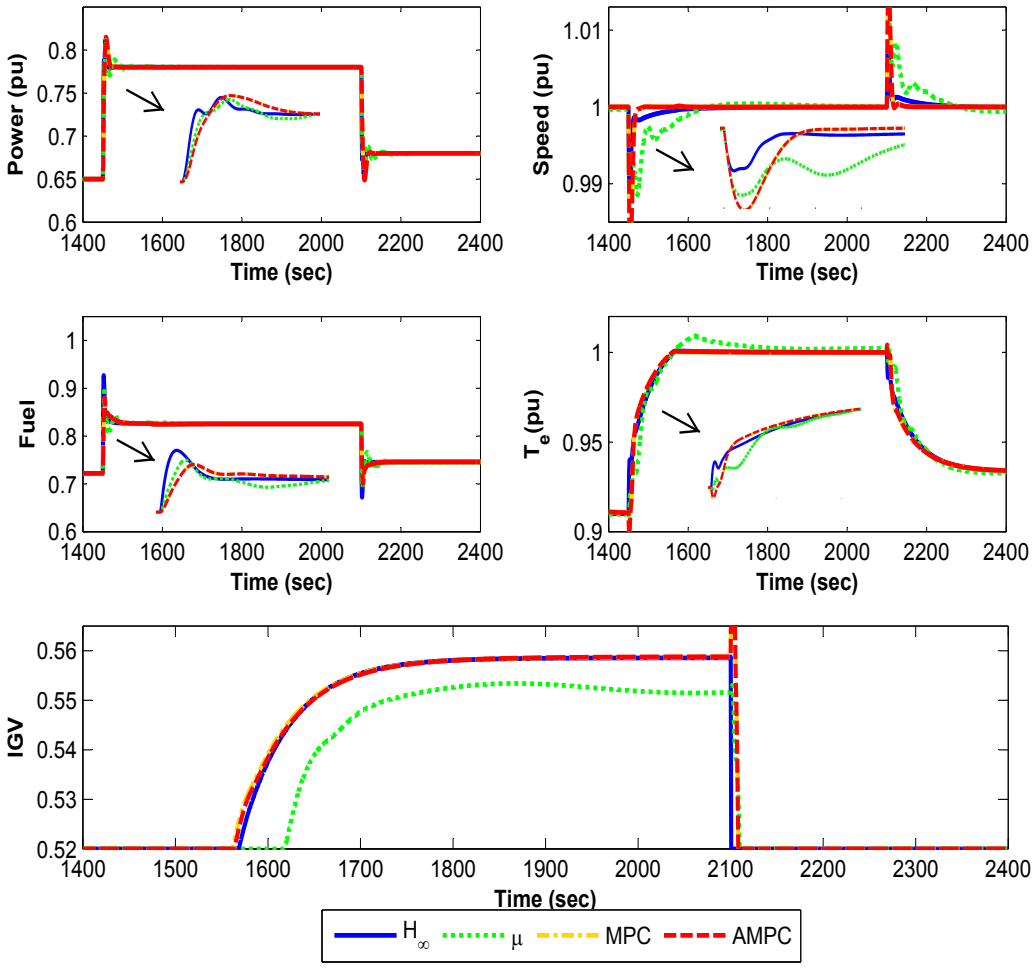

Figure 8: Control and output responses for the different controllers under nominal conditions

Table 2: Optimum time indices for MPC, AMPC, H_∞, and $\mu - synthesis$ controllers without model uncertainties

Output	$\mathbf{M}_P$ (%)	$\mathbf{T}_r(sec)$	$\mathbf{T}_s(sec)$	**Output**	$\mathbf{M}_P$ (%)	$\mathbf{T}_r(sec)$	$\mathbf{T}_s(sec)$
MPC				$\boldsymbol{H_\infty}$			
Power	26.79	2.93	68.96	Power	24.25	**1.40**	**62.69**
T_e	**0.36**	**65.88**	**150.05**	T_e	0.96	79.24	155.59
AMPC				$\boldsymbol{\mu}$			
Power	26.97	2.96	68.87	Power	**21.18**	2.31	93.58
T_e	0.78	**66.17**	**150.12**	T_e	10.24	80.21	600

Table 3: Error indices for MPC, AMPC, H_∞, and $\mu - synthesis$ controllers without model uncertainty

Error	**ISE**	**IAE**	**ITSE**	**ITAE**	**Error**	**ISE**	**IAE**	**ITSE**	**ITAE**
MPC					$\boldsymbol{H_\infty}$				
Power	8.81×10^{-01}	7.10	1257	10133	Power	$\mathbf{8.62 \times 10^{-01}}$	**6.81**	**1229**	**9721**
T_e	5.27×10^{-01}	**7.13**	756	**10307**	T_e	$\mathbf{5.09 \times 10^{-01}}$	7.26	**729**	10527
N	2.68×10^{-03}	**0.19**	3.90	281	N	$\mathbf{7.39 \times 10^{-04}}$	0.23	**1.08**	356
AMPC					$\boldsymbol{\mu}$				
Power	8.81×10^{-01}	7.10	1257	10134	Power	8.71×10^{-01}	7.14	1242	10214
T_e	5.26×10^{-01}	7.15	755	10350	T_e	5.92×10^{-01}	9.46	853	14139
N	2.66×10^{-03}	**0.19**	3.87	**277**	N	4.94×10^{-03}	0.80	7.31	1226

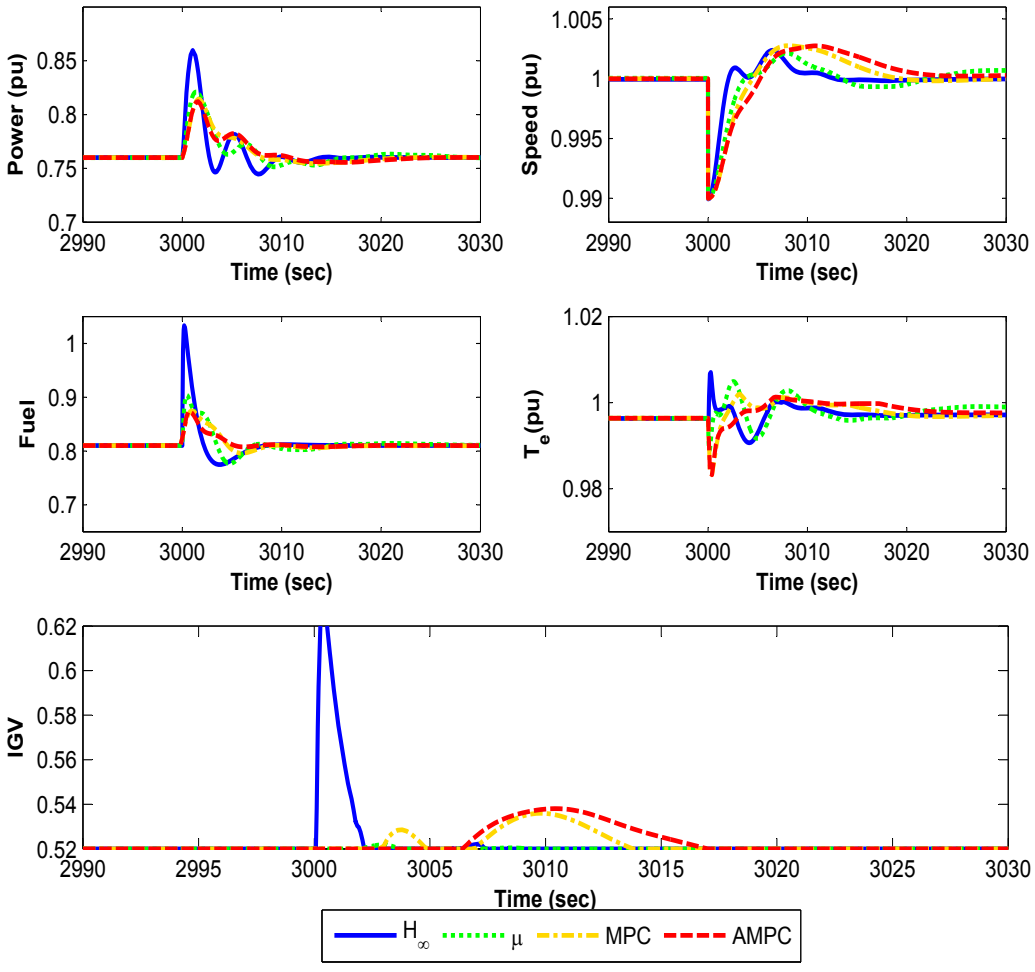

Figure 9: Control and output responses of the different controllers for 1% frequency drop and under nominal conditions

5.2. Nonlinear gas turbine response in the presence of low levels of model uncertainties

The dynamic responses and optimum time indices of the GTPP in the presence of a low model uncertainty are provided in Fig. 10 and Tables 5 and 6, respectively. Low levels of uncertainties are applied to the plant by changing the gain of the gas turbine fuel system from 1 to 2.

As Fig. 10 and Table 5 shows, AMPC and MPC controllers present the best rise time and settling time for temperature output compared with other

Table 4: ISE, IAE, ITSE, ITAE, mean, standard deviation (SD) and maximum deviation (MD) of output errors for 1% frequency drop without model uncertainty

Method	ISE	IAE	ITSE	ITAE	Mean	SD	MD
$\boldsymbol{H_\infty}$							
Power	1.34×10^{-02}	0.246	40.101	739	**0.756**	1.53×10^{-02}	9.97×10^{-02}
T_e	$\mathbf{1.55 \times 10^{-04}}$	**0.057**	**0.466**	**171**	**0.995**	$\mathbf{1.80 \times 10^{-03}}$	1.06×10^{-02}
N	$\mathbf{1.05 \times 10^{-04}}$	**0.023**	**0.316**	**69**	**1.000**	2.64×10^{-03}	2.38×10^{-03}
IGV	8.40×10^{-03}	0.112	25.213	337	**0.517**	1.43×10^{-02}	1.12×10^{-01}
Fuel	3.84×10^{-02}	0.355	115.115	1066	**0.801**	4.70×10^{-02}	2.23×10^{-01}
μ							
Power	7.34×10^{-03}	0.242	22.037	726	**0.756**	1.38×10^{-02}	6.10×10^{-02}
T_e	3.14×10^{-04}	0.088	0.946	264	**0.995**	2.24×10^{-03}	8.51×10^{-03}
N	1.52×10^{-04}	0.041	0.455	124	**1.000**	$\mathbf{2.00 \times 10^{-03}}$	$\mathbf{2.16 \times 10^{-03}}$
IGV	$\mathbf{2.86 \times 10^{-06}}$	**0.002**	**0.009**	**7**	0.520	$\mathbf{2.61 \times 10^{-04}}$	$\mathbf{1.82 \times 10^{-03}}$
Fuel	1.46×10^{-02}	0.335	43.787	1007	0.807	1.94×10^{-02}	9.33×10^{-02}
$\boldsymbol{MPC}$							
Power	6.44×10^{-03}	0.231	19.348	694	**0.756**	1.22×10^{-02}	5.44×10^{-02}
T_e	2.92×10^{-04}	0.074	0.877	224	**0.995**	2.34×10^{-03}	5.63×10^{-03}
N	2.16×10^{-04}	0.047	0.648	142	**1.000**	2.43×10^{-03}	2.76×10^{-03}
IGV	9.05×10^{-04}	0.078	2.724	234	0.518	4.35×10^{-03}	1.60×10^{-02}
Fuel	8.7×10^{-03}	0.236	26.108	710	0.807	1.45×10^{-02}	6.45×10^{-02}
$\boldsymbol{AMPC}$							
Power	$\mathbf{5.69 \times 10^{-03}}$	**0.223**	**17.087**	**671**	**0.756**	$\mathbf{1.13 \times 10^{-02}}$	$\mathbf{5.21 \times 10^{-02}}$
T_e	3.28×10^{-04}	0.092	0.988	279	**0.995**	2.32×10^{-03}	$\mathbf{4.89 \times 10^{-03}}$
N	2.33×10^{-04}	0.058	0.701	174	**1.000**	2.51×10^{-03}	2.75×10^{-03}
IGV	1.56×10^{-03}	0.113	4.706	341	**0.517**	5.59×10^{-03}	1.81×10^{-02}
Fuel	$\mathbf{5.81 \times 10^{-03}}$	**0.168**	**17.448**	**505**	0.807	$\mathbf{1.16 \times 10^{-02}}$	$\mathbf{6.29 \times 10^{-02}}$

controllers. Furthermore, as Table 6 shows, AMPC strategy provides the best ISE, IAE, and ITAE error for temperature output. From Fig. 10 it can be seen that by applying model uncertainty to GTPP, in the case of H_∞, there are some oscillations in the IGV control signal. Although these oscillations are limited, they can negatively affect H_∞ control performance and, as consequence the performance of GTPP. As Fig. 10 and Table 5 show, a sudden increase in fuel flow leads to overshoots in MPC and AMPC outputs. In the case of speed output, based on the Table 6, H_∞ presents the best control performance.

Figure 11 and Table 7 depict the gas turbine plant responses for a 1% instantaneous speed (frequency) deviation. As this figure and Table show, the AMPC strategy provides the best fuel control signal and power output. Also, it can provides a lower overshoot in fuel control signal, and especially temperature, power and speed outputs. Based on Fig. 11, H_∞ shows a high level of overshoot for temperature, speed, IGV, power demand, and fuel flow signals. Although an effective action of H_∞ leads to a minimum error for speed output, as Table 7 shows, in a real power plant a high level of overshoot in any output can be unacceptable and lead to serious problems. In Table 7, the minimum error for temperature output belongs to MPC controller.

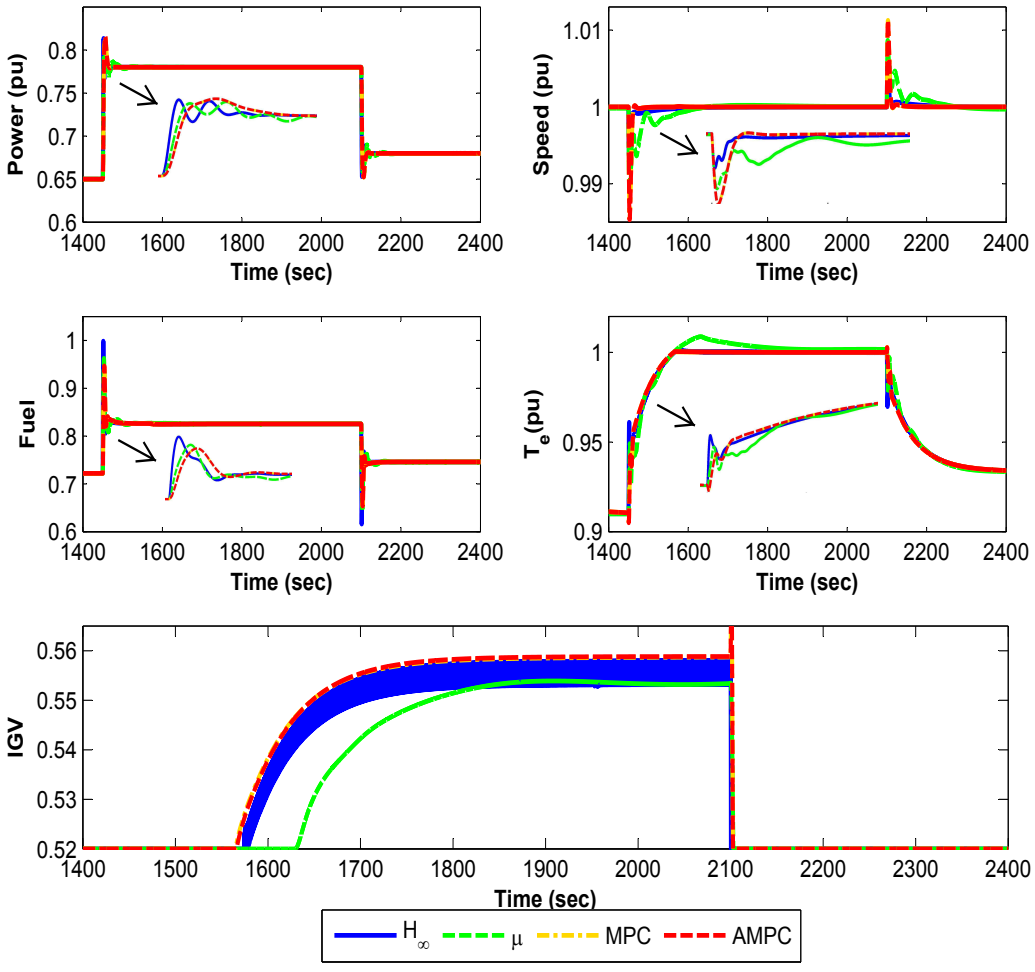

Figure 10: Control and output responses for different controllers in the presence of low levels of model uncertainties

Table 5: Optimum time indices for MPC, AMPC, H_∞, and $\mu - synthesis$ controllers with low model uncertainty

Output	$\mathbf{M}_P$ (%)	$\mathbf{T}_r(sec)$	$\mathbf{T}_s(sec)$	**Output**	$\mathbf{M}_P$ (%)	$\mathbf{T}_r(sec)$	$\mathbf{T}_s(sec)$
MPC				$\boldsymbol{H_\infty}$			
Power	27.32	1.63	63.45	Power	25.83	**0.86**	**60.37**
T_e	**0.34**	**74.95**	**153.70**	T_e	1.76	79.61	156.56
AMPC				$\boldsymbol{\mu}$			
Power	27.57	1.65	63.51	Power	**22.41**	1.41	89.71
T_e	0.63	**74.90**	**153.67**	T_e	9.85	81.11	468.65

Table 6: Error indices for MPC, AMPC, H_∞, and $\mu - synthesis$ controllers with low model uncertainty

Error	**ISE**	**IAE**	**ITSE**	**ITAE**	**Error**	**ISE**	**IAE**	**ITSE**	**ITAE**
MPC					$\boldsymbol{H_\infty}$				
Power	8.74×10^{-01}	6.95	1246	9917	Power	$\mathbf{8.58 \times 10^{-01}}$	**6.74**	**1223**	**9613**
T_e	$\mathbf{4.95 \times 10^{-01}}$	**7.00**	709	10124	T_e	$\mathbf{4.94 \times 10^{-01}}$	7.10	**707**	10279
N	9.38×10^{-04}	**0.096**	1.36	**140**	N	$\mathbf{2.10 \times 10^{-04}}$	0.12	**0.31**	178
AMPC					$\boldsymbol{\mu}$				
Power	8.74×10^{-01}	6.95	1246	9921	Power	8.64×10^{-01}	6.97	1232	9954
T_e	$\mathbf{4.95 \times 10^{-01}}$	**6.99**	710	**10106**	T_e	5.35×10^{-01}	8.94	770	13372
N	9.50×10^{-04}	**0.10**	1.38	141	N	1.40×10^{-03}	0.40	2.06	614

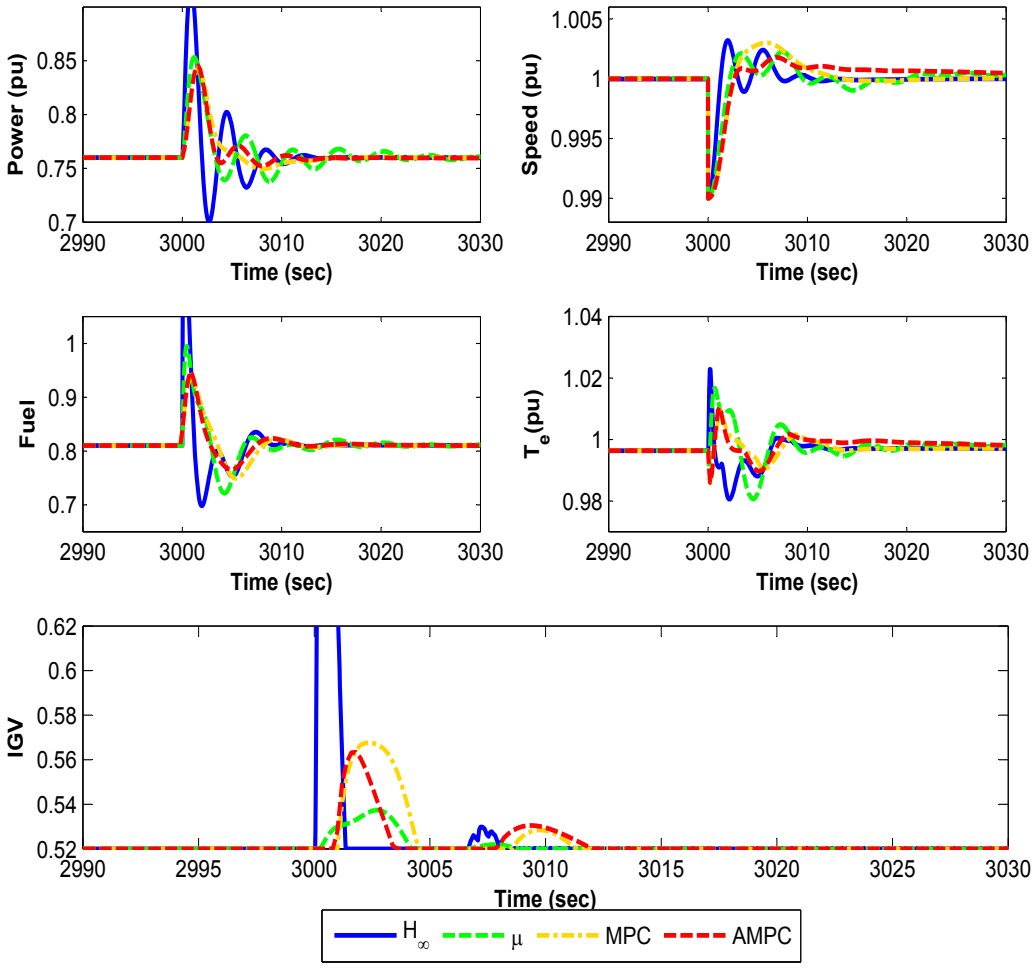

Figure 11: Control and output responses of the different controllers for 1% frequency drop and low levels of model uncertainties

5.3. Nonlinear gas turbine response in the presence of high levels of model uncertainties

The dynamic responses and optimum time indices of the gas turbine power plant at the presence of a high model uncertainty for the MPC, AMPC, H_∞, and $\mu - synthesis$ controllers are illustrated in Fig. 12 and Tables 8 and 9. The uncertainty is applied to the plant by increasing the gain of the gas turbine fuel system from 1 to 3.0.

Table 7: ISE, IAE, ITSE, ITAE, mean, standard deviation (SD) and maximum deviation (MD) of output errors for 1% frequency drop with low model uncertainty

Method	ISE	IAE	ITSE	ITAE	Mean	SD	MD
$\boldsymbol{H_\infty}$							
Power	2.94×10^{-02}	0.363	88.129	1090	**0.756**	$\mathbf{1.53 \times 10^{-02}}$	1.61×10^{-01}
T_e	6.07×10^{-04}	0.079	1.822	239	**0.996**	$\mathbf{2.23 \times 10^{-03}}$	2.64×10^{-02}
N	$\mathbf{8.13 \times 10^{-05}}$	**0.018**	**0.244**	**55**	**1.000**	1.44×10^{-03}	3.21×10^{-03}
IGV	$\mathbf{5.61 \times 10^{-02}}$	0.245	168.348	737	0.518	1.90×10^{-02}	3.21×10^{-01}
Fuel	1.19×10^{-01}	0.615	357.894	1847	**0.805**	4.17×10^{-02}	4.42×10^{-01}
$\boldsymbol{\mu}$							
Power	1.42×10^{-02}	0.335	42.656	1008	**0.756**	1.85×10^{-02}	9.32×10^{-02}
T_e	1.03×10^{-03}	0.122	3.100	368	**0.995**	4.87×10^{-03}	2.03×10^{-02}
N	1.16×10^{-04}	0.031	0.347	94	**1.000**	1.90×10^{-03}	2.26×10^{-03}
IGV	5.93×10^{-04}	**0.047**	**1.782**	**141**	0.519	$\mathbf{3.66 \times 10^{-03}}$	$\mathbf{1.74 \times 10^{-02}}$
Fuel	4.47×10^{-02}	0.528	134.141	1586	0.806	3.56×10^{-02}	1.85×10^{-01}
$\boldsymbol{MPC}$							
Power	1.13×10^{-02}	0.238	33.839	716	**0.756**	1.64×10^{-02}	$\mathbf{8.33 \times 10^{-02}}$
T_e	$\mathbf{2.92 \times 10^{-04}}$	**0.065**	**0.878**	**195**	**0.996**	2.55×10^{-03}	$\mathbf{1.33 \times 10^{-02}}$
N	1.70×10^{-04}	0.035	0.510	106	**1.000**	2.18×10^{-03}	3.00×10^{-03}
IGV	4.91×10^{-03}	0.135	14.752	406	**0.517**	1.06×10^{-02}	4.76×10^{-02}
Fuel	3.07×10^{-02}	0.454	92.144	1365	0.807	2.76×10^{-02}	$\mathbf{1.25 \times 10^{-01}}$
$\boldsymbol{AMPC}$							
Power	$\mathbf{1.04 \times 10^{-02}}$	**0.205**	**31.110**	**615**	**0.756**	1.57×10^{-02}	8.54×10^{-02}
T_e	4.35×10^{-04}	0.106	1.308	320	**0.995**	2.73×10^{-03}	1.42×10^{-02}
N	1.51×10^{-04}	0.042	0.453	125	**1.000**	2.06×10^{-03}	1.79×10^{-03}
IGV	2.49×10^{-03}	0.095	7.472	286	0.518	7.54×10^{-03}	4.34×10^{-02}
Fuel	$\mathbf{2.58 \times 10^{-02}}$	**0.391**	**77.560**	**1175**	0.807	$\mathbf{2.52 \times 10^{-02}}$	1.38×10^{-01}

As Fig. 12 and Table 8 show, the AMPC controller provides the best minimum overshoot for power output, also this controller improves temperature output for GTPP. As this figure and Table show, by increasing the uncertainty, all outputs experience a high level of overshoot, however this is especially severe for $\mu - synthesis$ and H_∞ controllers. Based on Table 9, H_∞ controller provides the lowest power demand output error, while MPC controller provides a better responses in speed and temperature outputs.

As Fig. 13 and Table 10 shows for 1٪ frequency deviation, by increasing uncertainty, similar to H_∞ and $\mu - sunthesis$ cases, the maximum overshoot for all outputs controlled by MPC controller will increase dramatically. Here, the noticeable results is that, compared with MPC, H_∞, and $\mu - sunthesis$ controller, AMPC controller can tolerate a wider range of uncertainties. This is mainly because AMPC controller uses an online parameter estimation to follow any change in GTPP model, and then updates the control rules based on the new identified model. As Table 10 shows, AMPC controller provides the best power, fuel flow, and temperature signals. As figure shows, the $\mu - sunthesis$ controller experiences some oscillations in power, speed, temperature and fuel flow signals. Considering the stability of IGV signal, it can be concluded that these oscillations are in a direct connection with speed loop and especially fuel control system. Based on Fig. 13, although H_∞ provides the best minimum error for speed output N, considering maximum overshoot, the outputs provided by AMPC seem to be more reasonable. The AMPC strategy provides the lowest overshoot for power, temperature, and speed outputs, and also fuel flow control signal.

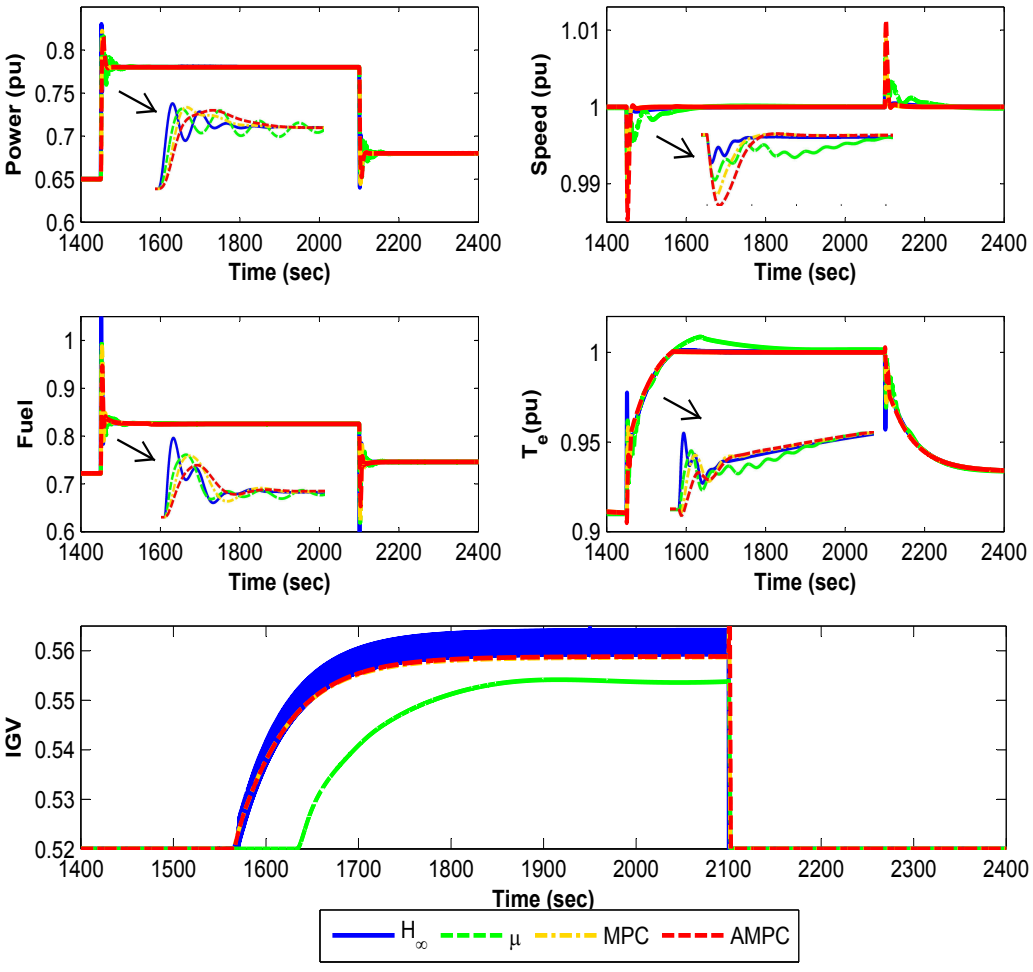

Figure 12: Control and output responses for different controllers in the presence of high levels of model uncertainties

Table 8: Optimum time indices for MPC, AMPC, H_∞, and $\mu - synthesis$ controllers with high model uncertainty

Output	$\mathbf{M}_P$ (%)	$\mathbf{T}_r(sec)$	$\mathbf{T}_s(sec)$	**Output**	$\mathbf{M}_P$ (%)	$\mathbf{T}_r(sec)$	$\mathbf{T}_s(sec)$
MPC				$\boldsymbol{H_\infty}$			
Power	32.41	1.26	62.17	Power	38.46	**0.66**	**58.77**
T_e	**0.35**	76.70	154.83	T_e	1.16	79.72	156.88
AMPC				$\boldsymbol{\mu}$			
Power	**27.57**	1.65	63.51	Power	29.72	1.07	89.61
T_e	0.63	**74.90**	**153.67**	T_e	9.65	80.77	462.68

Table 9: Error indices for MPC, AMPC, H_∞, and $\mu - synthesis$ controllers with high model uncertainty

Error	**ISE**	**IAE**	**ITSE**	**ITAE**	**Error**	**ISE**	**IAE**	**ITSE**	**ITAE**
MPC					$\boldsymbol{H_\infty}$				
Power	8.71×10^{-01}	6.88	1241	9821	Power	$\mathbf{8.57 \times 10^{-01}}$	**6.73**	**1222**	**9591**
T_e	$\mathbf{4.87 \times 10^{-01}}$	**6.95**	**697**	**10064**	$\boldsymbol{T_e}$	4.89×10^{-01}	7.10	701	10302
N	4.87×10^{-04}	**0.06**	**0.71**	**93**	N	$\mathbf{1.00 \times 10^{-04}}$	0.08	1.47	119
AMPC					$\boldsymbol{\mu}$				
Power	8.74×10^{-01}	6.95	1246.32	9921	Power	8.64×10^{-01}	7.01	1232	10007
T_e	4.95×10^{-01}	6.99	710	10106	T_e	5.19×10^{-01}	8.74	746	13074
N	9.50×10^{-04}	0.10	1.38	141	N	6.68×10^{-04}	0.27	0.98	412

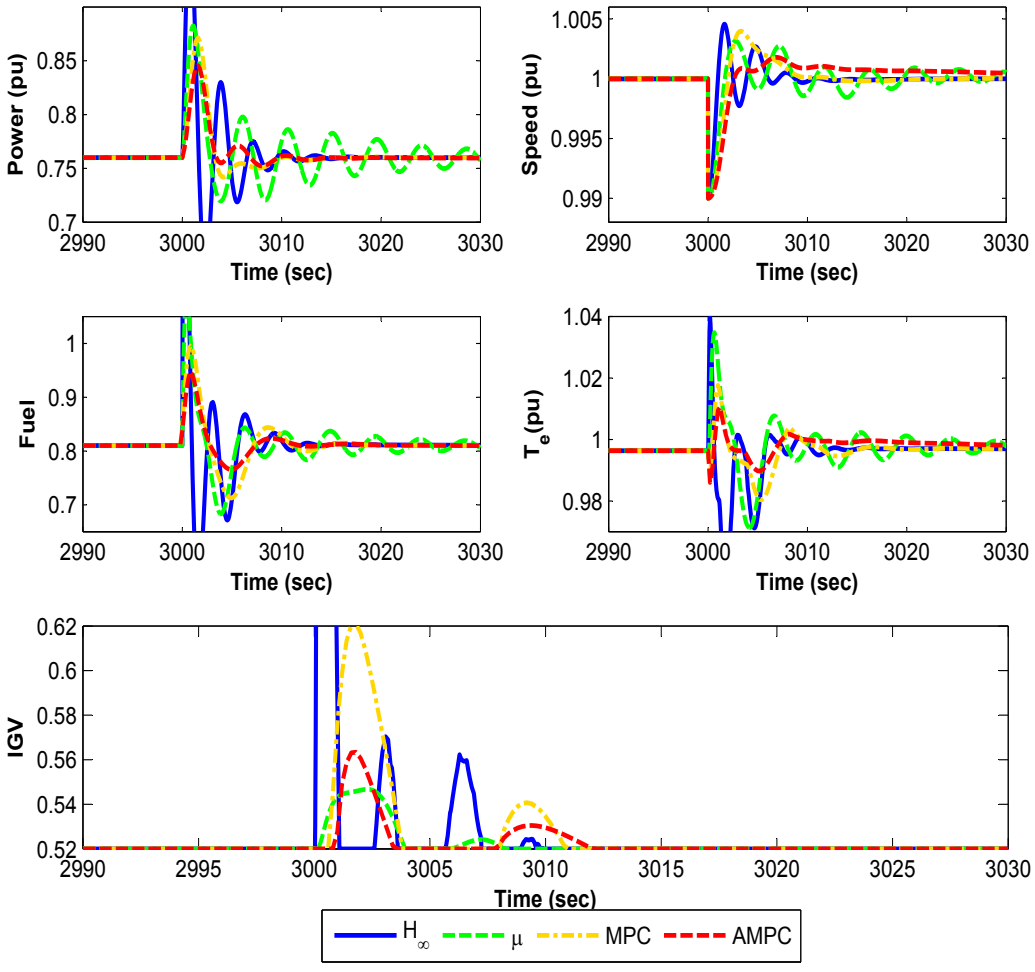

Figure 13: Control and output responses of the different controllers for 1% frequency drop and high levels of model uncertainties

Overall, considering all three applied uncertainties to the V94.2 GTPP, and all controllers' results, it can be concluded that though under nominal conditions it is hard to distinguish the difference in performance between all controllers, when uncertainties are introduced to the systems, the superior performance of AMPC became apparent, especially as uncertainties increased in magnitude. AMPC controller uses an online parameter estimation and adaptive mechanism to follow any change in V94.2 GTPP model and provide the best control performance possible.

Table 10: ISE, IAE, ITSE, ITAE, mean, standard deviation (SD) and maximum deviation (MD) of output errors for 1% frequency drop with high model uncertainty

Method	**ISE**	**IAE**	**ITSE**	**ITAE**	**Mean**	**SD**	**MD**
$\boldsymbol{H_\infty}$							
Power	4.88×10^{-02}	0.468	146.350	1407	0.759	3.64×10^{-02}	2.11×10^{-01}
T_e	2.86×10^{-03}	0.130	8.580	392	0.997	8.36×10^{-03}	4.32×10^{-02}
N	$\mathbf{7.95 \times 10^{-05}}$	**0.019**	**0.239**	**56**	**1.000**	2.39×10^{-03}	4.57×10^{-03}
IGV	1.26×10^{-01}	0.394	378.484	1183	**0.509**	5.80×10^{-02}	4.81×10^{-01}
Fuel	2.69×10^{-01}	1.000	808.711	3004	**0.792**	1.02×10^{-01}	6.60×10^{-01}
$\boldsymbol{\mu}$							
Power	2.63×10^{-02}	0.613	78.953	1846	**0.756**	2.51×10^{-02}	1.22×10^{-01}
T_e	2.38×10^{-03}	0.173	7.137	521	**0.995**	7.53×10^{-03}	3.84×10^{-02}
N	1.15×10^{-04}	0.035	0.346	107	**1.000**	$\mathbf{1.91 \times 10^{-03}}$	3.14×10^{-03}
IGV	$\mathbf{1.67 \times 10^{-03}}$	**0.079**	**5.014**	**236**	0.518	$\mathbf{6.05 \times 10^{-03}}$	$\mathbf{2.67 \times 10^{-02}}$
Fuel	8.32×10^{-02}	0.852	249.890	2564	0.805	4.78×10^{-02}	2.74×10^{-01}
$\boldsymbol{MPC}$							
Power	1.77×10^{-02}	0.268	53.056	805	**0.756**	2.07×10^{-02}	1.11×10^{-01}
T_e	8.60×10^{-04}	**0.096**	2.583	**288**	0.996	4.63×10^{-03}	2.13×10^{-02}
N	1.53×10^{-04}	0.030	0.459	91	**1.000**	2.08×10^{-03}	3.97×10^{-03}
IGV	1.58×10^{-02}	0.234	47.577	704	0.514	1.91×10^{-02}	1.01×10^{-01}
Fuel	6.33×10^{-02}	0.682	190.043	2049	0.807	3.98×10^{-02}	1.85×10^{-01}
$\boldsymbol{AMPC}$							
Power	$\mathbf{1.04 \times 10^{-02}}$	**0.205**	**31.110**	**615**	**0.756**	$\mathbf{1.57 \times 10^{-02}}$	$\mathbf{8.54 \times 10^{-02}}$
T_e	$\mathbf{4.35 \times 10^{-04}}$	0.106	**1.308**	320	**0.995**	$\mathbf{2.73 \times 10^{-03}}$	$\mathbf{1.42 \times 10^{-02}}$
N	1.51×10^{-04}	0.042	0.453	125	**1.000**	2.06×10^{-03}	$\mathbf{1.79 \times 10^{-03}}$
IGV	2.49×10^{-03}	0.095	7.472	286	0.518	7.54×10^{-03}	4.34×10^{-02}
Fuel	$\mathbf{2.58 \times 10^{-02}}$	**0.391**	**77.560**	**1175**	0.807	$\mathbf{2.52 \times 10^{-02}}$	$\mathbf{1.38 \times 10^{-01}}$

6. Conclusions

In this paper, an AMPC controller has been designed and successfully implemented to the speed and temperature control loops of a V94.2 gas turbine power plant. This controller used online parameters estimation to compensate for any difference between the estimated ARX linear model and the main gas turbine nonlinear model. The performance and effectiveness of the proposed AMPC controller has been assessed compared to H_∞ and $\mu - synthesis$ robust control strategies and an MPC controller. The simulations and analyses clearly showed that the online parameters estimation procedure can assist AMPC controller to follow any change or compensate any inconsistency in the model parameters. Finally, though all the controllers were able to improve the gas turbine's speed and temperature output responses, the AMPC controller outperformed all the other approaches in terms of transient and steady-state responses, disturbance rejection properties, and robustness performance, especially as model uncertainty levels increased.

References

[1] Haji Haji V, Fekih, A, Monje CA, Fakhri Asfestani R, H_2, H_∞, H_2/H_∞ and $\mu - synthesis$ controllers for the speed and temperature control of a real gas turbine unit in a combined cycle power plant, Energy Science & Engineering 2019:2205–2222.

[2] Haji Haji V, Fekih A, Monje CA, H_∞ robust control design for a combined cycle power plant, 2019 IEEE PES GTD Grand International Conference and Exposition Asia (GTD Asia), 2019: 384–389.

[3] Eslami M, Shayesteh MR, Pourahmadi M, Optimal design of PID-based low-pass filter for gas turbine using intelligent method, IEEE Access 2018;6:15335–15345.

[4] Haji Haji V, Monje CA, Fractional order fuzzy-PID control of a combined cycle power plant using particle swarm optimization algorithm with an improved dynamic parameters selection. Appl Soft Comput 2017;58:256–264.

[5] Sung SW, Lee IB, Limitations and countermeasures of PID controllers. Ind Eng Chem Res 1996;35,2596–2610.

[6] Raković SV, Levine WS, Handbook of model predictive control, Springer, 2019.

[7] Camacho EF, Bordons C, Model predictive control in the process industry, Springer-Verlag London, 1995.

[8] Bordons C, Garcia-Torres F, Ridao M, Model predictive control of microgrids, Springer International Publishing, 2020.

[9] Bracco G, Canale M, Cerone V, Optimizing energy production of an inertial sea wave energy converter via model predictive control. Control Eng Pract 2020;96. https://doi.org/10.1016/j.conengprac.2020.104299.

[10] Liu W, Liu Y, Hierarchical model predictive control of wind farm with energy storage system for frequency regulation during black-start, Int J Elec Power 2020;119. https://doi.org/10.1016/j.ijepes.2020.105893.

[11] Shan K, Fan C, Wang J, Model predictive control for thermal energy storage assisted large central cooling systems, Energy 2019;179:916–927.

[12] Ghorbani H, Ghaffari A, Rahnama M, Constrained model predictive control implementation for a heavy-duty gas turbine power plant. WSEAS Transactions on Systems and Control 2008;3:507–516.

[13] Rowen WI, Simplified mathematical representation of heavy-duty gas turbines. J Eng Gas Turbines Power 1983;105:865–9.

[14] Rowen WI, Simplified mathematical representation of single shaft gas turbines in mechanical drive service. In: international gas turbine and aeroengine congress and exposition cologne, Germany. 1992.

[15] Kunitomi K et al., Modeling frequency dependency of gas turbine output. In: IEEE Power Engineering Society Winter Meeting, 2001, pp. 678–683.

[16] Balamurugan S, Janarthanan N, Vijaya Chandrakala KRM, Small and large signal modeling of heavy duty gas turbine plant for load frequency control, Electrical Power and Energy Systems 2016;79:84–88.

[17] Mehrpanahi A, Payganeh G, Arbabtafti M, Dynamic modeling of an industrial gas turbine in loading and unloading conditions using a gray box method, Energy 2016;1–13.

[18] Kakimoto N, Baba K, Performance of gas turbine-based plants during frequency drops, IEEE Trans Power Syst 2003;18:1110–1115.

[19] Mantzaris J, Vournas C, Modeling and stability of a single-shaft combined cycle power plant, Int J Thermo 2007;10:71–78.

[20] Camacho EF, Bordon C, Model Predictive control. Springer, Verlag London, 2007.

[21] Bemporad A, Manfred M, Ricker NL, Model predictive control toolbox. The MathWorks, Inc., 2015.

[22] Slotine JJE, Li W, Applied nonlinear control, Prentice-Hall Inc, 1991.

[23] Haji Haji V, Monje CA, Fractional-order PID control of a MIMO distillation column process using improved bat algorithm. Soft Comput 2019;23:8887–8906.